Available online at www.sciencedirect.com
ScienceDirect
C. R. Physique 8 (2007) 180–198
COMPTES RENDUS PHYSIQUE
http://france.elsevier.com/direct/COMREN/

Recent advances in crystal optics/Avancées récentes en optique cristalline

Quasi-phasematching

David S. Hum *, Martin M. Fejer

E.L. Ginzton Laboratory, Stanford University, Stanford, CA 94305, USA

Available online 30 November 2006

Invited paper

Abstract

The use of microstructured crystals in quasi-phasematched (QPM) nonlinear interactions has enabled operation of nonlinear devices in regimes inaccessible to conventional birefringently phasematched media. This review addresses basic aspects of the theory of QPM interactions, microstructured ferroelectrics and semiconductors for QPM, devices based on QPM media, and a series of techniques based on engineering of QPM gratings to tailor spatial and spectral response of QPM interactions. Because it is not possible in a brief review to do justice to the large body of results that have been obtained with QPM media over the past twenty years, the emphasis in this review will be on aspects of QPM interactions beyond their use simply as highly nonlinear alternatives to conventional birefringent media. ***To cite this article: D.S. Hum, M.M. Fejer, C. R. Physique 8 (2007).***

Résumé

Quasi-accord de phase. L'utilisation de cristaux microstructurés pour les interactions optiques non linéaires en quasi-accord de phase (QAP) a permis le fonctionnement de dispositifs non linéaires dans des régimes inaccessibles avec des milieux biréfringents conventionnels en accord de phase. Cette revue traite de la théorie de base des interactions en QAP, des ferroélectriques et semiconducteurs microstructurés pour le QAP, des dispositifs basés sur les milieux à QAP, ainsi que d'une série de techniques basées sur l'ingénierie des réseaux de QAP dans l'objectif de façonner les réponses, spatiale et spectrale, des interactions en QAP. Comme il n'est pas possible de rendre justice en une brève revue au grand nombre de résultats qui ont été obtenus pour les milieux à quasi-accord de phase au cours des vingt dernières années, la présente contribution se concentrera sur quelques aspects des interactions en QAP au-delà de leur simple utilisation comme alternatives hautement non linéaires aux milieux conventionnels biréfringents. ***Pour citer cet article : D.S. Hum, M.M. Fejer, C. R. Physique 8 (2007).***

1. Overview and early history

Efficient quadratic nonlinear optical interactions require that the relative phase between the interacting waves be maintained. The phase drift naturally resulting from the difference in phase velocities due to material dispersion must be compensated by some phasematching means. For the first twenty-five years of nonlinear optics, the dominant method employed was birefringent phasematching (BPM), in which the difference in phase velocity of orthogonally polarized waves was used to balance the difference due to dispersion. An alternative approach, quasi-phasematching

* Corresponding author.
E-mail addresses: dhum@stanford.edu (D.S. Hum), fejer@stanford.edu (M.M. Fejer).

1631-0705/$ – see front matter
doi:10.1016/j.crhy.2006.10.022

(QPM), uses a periodic modification of the properties of the nonlinear medium to correct the relative phase at regular intervals without matching phase velocities. A particularly effective structure is one in which the sign of the nonlinear susceptibility is periodically reversed throughout the medium. While QPM was actually invented prior to birefringent phasematching [1,2], it did not see widespread use due to difficulties in fabricating suitable crystals with the required micron-scale structures. The advent and rapid evolution of lithographically controlled patterning of nonlinear media beginning in the late 1980s led to widespread use of QPM media, which have opened up new operating regimes for nonlinear interactions. QPM has a role both as a more efficient way to accomplish functions available in homogeneous media, and as a way to implement functions unavailable in conventional media.

2. QPM basics

2.1. QPM second harmonic generation

In this discussion, second harmonic generation (SHG) will be used as a prototypical interaction for simplicity. The essential results that emerge are applicable to other interactions; key differences are pointed out as they arise.

In SHG, a plane wave field of amplitude E_1 at frequency ω_1 and wavevector $k_1 = n_1\omega_1/c$, where n_1 is the refractive index, passes through a medium with quadratic nonlinear susceptibility d, generating a nonlinear polarization wave proportional to dE_1^2 at frequency $\omega_2 = 2\omega_1$ and wavevector $2k_1$. The polarization wave radiates a free second harmonic wave with wave vector $k_2 = n_2\omega_2/c$. The forced and free waves accumulate a phase shift of π over a distance known as the coherence length, $l_c = \pi/(k_2 - 2k_1) = \lambda/4(n_2 - n_1)$, where λ is the vacuum wavelength of the fundamental wave. The direction of power flow between the fundamental and harmonic depends on the relative phase of the forced and free waves, and hence changes sign every coherence length. By changing the sign of the nonlinear susceptibility every coherence length, the phase of the polarization wave is shifted by π, effectively rephasing the interaction and leading to monotonic power flow into the harmonic wave, as illustrated in Fig. 1.

As can be seen in Fig. 1, the average growth rate of the QPM harmonic wave is lower than that of a phasematched wave in the same medium, but QPM processes have several advantages that frequently more than offset this factor. As the QPM process does not rely on birefringence, any convenient choice of polarizations can be used, including the case of all waves polarized parallel to one another (inaccessible to birefringently phasematched interactions), which couples to the largest component of the nonlinear susceptibility tensor in common ferroelectrics like $LiNbO_3$. It is even possible to operate in isotropic media like GaAs in which BPM is not possible. For similar reasons, it is always possible to use QPM for waves propagating along a crystal axis, eliminating the Poynting-vector walkoff that reduces the efficiency of critically phasematched interactions in birefringent media. The use of gratings that are not simply periodic in either the propagation or transverse directions allows tailoring of the nonlinear interaction in ways that are not possible in BPM media (Section 5). From a materials engineering standpoint, QPM allows one or a few materials to serve as a systematically engineerable platform for a large variety of device applications, a simplification that holds significant practical advantage over developing a large number of different BPM media for use in a variety of low-volume applications.

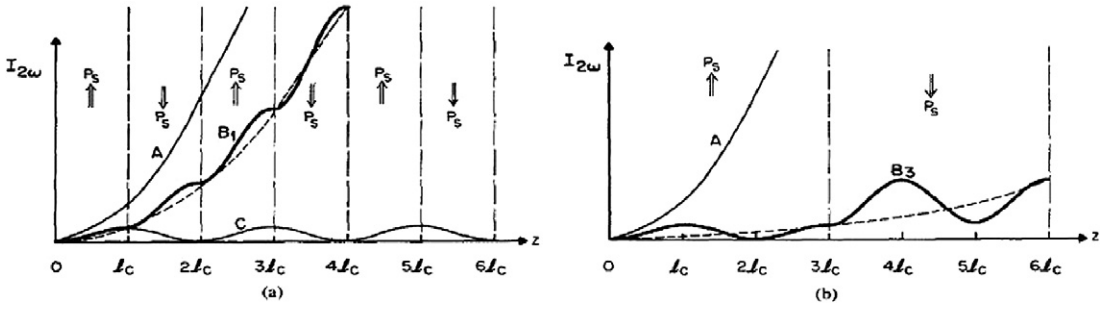

Fig. 1. Effect of phase matching on the growth of second harmonic intensity with distance in a nonlinear crystal. (a) *A*: perfect phasematching in a uniformly poled crystal; *C*: non-phasematched interaction; *B*: first-order QPM by flipping the sign of the spontaneous polarization every coherence length of the interaction of curve C. (b) *A*: perfect phasematching; *B*: third-order QPM by flipping the polarization every three coherence lengths.

2.2. Theory of SHG in ideal QPM medium

To quantify some of the basic considerations for QPM interactions, consider the simplest possible case, plane-wave SHG with an undepleted continuous-wave pump field. The analysis is similar to that in Ref. [3], in which a much more detailed treatment is available. The slowly-varying envelope equation for the evolution of the second harmonic field is

$$\mathrm{d}E_2/\mathrm{d}z = \Gamma d(z)\mathrm{e}^{-\mathrm{i}\Delta k' z} \tag{1}$$

where $\Gamma \equiv \mathrm{i}\omega E_1^2/n_2 c$, $d(z)$ is the (possibly) spatially varying nonlinear susceptibility, and $\Delta k' = k_2 - 2k_1$. For a crystal of length L, this equation can be integrated trivially, yielding

$$E_2(L) = \Gamma \int_0^L d(z)\mathrm{e}^{-\mathrm{i}\Delta k' z}\,\mathrm{d}z \tag{2}$$

It is interesting to note that this form of the solution is proportional to the spatial Fourier transform of the nonlinear susceptibility. We will find this identification useful for both quantitative and intuitive description of many features of QPM interactions.

For a uniform medium, $d(z)$ is simply a "top hat" distribution of magnitude d_{eff} and length L. The solution is simply

$$E_2(L) = \mathrm{i}\exp^{-\mathrm{i}\Delta k' L/2}\,\Gamma L d_{\mathrm{eff}}\,\mathrm{sinc}(\Delta k' L/2) \tag{3}$$

where $\mathrm{sinc}(x) \equiv \sin(x)/x$. For a medium with a periodic modulation of the nonlinear susceptibility with period Λ and hence fundamental spatial frequency $K_g = 2\pi/\Lambda$, we can write the nonlinear susceptibility as a Fourier series,

$$d(z) = \sum_m d_m \mathrm{e}^{\mathrm{i}K_m z} \tag{4}$$

where the mth spatial harmonic $K_m = mK_g$, and d_m is the corresponding Fourier coefficient. With such a periodic medium, integrating Eq. (2) yields

$$E_2(L) = \mathrm{i}\exp^{-\mathrm{i}\Delta k L/2}\,\Gamma L d_m\,\mathrm{sinc}(\Delta k L) \tag{5}$$

where the effective phase mismatch is $\Delta k \equiv \Delta k' - K_m$ and we have assumed that one Fourier component of the QPM grating is sufficiently closer than the others to $\Delta k'$ to dominate the integral. It can be seen that under these assumptions, the periodically modulated medium yields the same result as a homogeneous medium, but with an effective nonlinear coefficient d_m and the phasematching peak shifted from $\Delta k' = 0$ to $\Delta k' = K_m$. For a square-wave modulation from $+d_{\mathrm{eff}}$ to $-d_{\mathrm{eff}}$ with duty cycle D, a standard Fourier series result yields

$$d_m = d_{\mathrm{eff}} 2\sin(\pi D)/m\pi \tag{6}$$

We see that the largest QPM nonlinear coefficient, obtained for $m = 1$ is reduced below that of a uniform medium by a factor $2/\pi$, and for mth order QPM a further reduction by a factor $1/m$ appears.

Note that from this analysis it is clear that any Fourier component of the QPM grating at the correct spatial frequency will contribute to a QPM interaction. While a sign reversal grating is the most effective, other forms, such as an "on-off" grating can also work, though with a smaller Fourier component ($1/m\pi$ in the case of an ideal on-off grating), and hence lower efficiency.

2.3. Imperfections

An important consideration for setting specifications for the fabrication of useful QPM media is the effect of imperfections in the QPM grating. These are discussed at length in Ref. [3]. Here we simply note some of the key results.

A common fabrication problem is the running together of adjacent domains. If a fraction f of the nominal domains are of the wrong orientation, the peak efficiency is reduced compared to the ideal structure by a factor of $(1 - 2f)^2$. Thus, 5% of the domains with the wrong orientation reduces the efficiency to 81% of nominal.

The case of random errors in domain size is more complex. Two limiting cases can be considered. "Period errors" are those as would result from the stacking of plates with a distribution of thicknesses with mean value l_c and variance σ_l^2. These errors accumulate in the manner of a random walk, so that the variance in the position of the Nth interface with respect to its nominal position is $N\sigma_l^2$. "Duty cycle errors" are those as would occur for a pattern whose long range order were set perfectly by, for example, a lithographic pattern, but the position of a given edge with respect to its nominal position has a variance of $\sigma_l^2/2$, so that the variance in the length of the domains is σ_l^2. The general analysis of these cases [3] is too complicated to enter into here; we give only the simplified result for $\hat{\eta}$, the efficiency normalized to the nominal efficiency, in the limit where the number of periods is large. For duty cycle errors, we find

$$\hat{\eta} \approx \exp\left(-\pi^2\sigma_l^2/2l_c^2\right) \tag{7}$$

while for period errors, with the additional assumption that the reduction is small

$$\langle\hat{\eta}\rangle \approx 1 - \frac{\pi^2}{6}N\frac{\sigma_l^2}{l_c^2} \tag{8}$$

From these we find that the tolerance for errors in duty cycle and period to retain 50% of nominal efficiency are $\sigma_l/l_c < 0.375$ and $\sigma_l/l_c < 0.72/\sqrt{N}$. It can be seen that the tolerance for duty cycle errors is rather loose, with variations in excess of $1/3$ the domain width reducing the efficiency by less than 50%, while the accumulating nature of the period errors leads to much more stringent criteria. For a structure 30-mm-long structure with 30-μm periods, $N = 2000$, and the tolerance is only $0.016\ l_c$. It is this strict tolerance for period errors that makes techniques based on lithographic patterning much more attractive than other fabrication methods.

It should be noted that these results are for behavior at the phasematching peak. For some applications, e.g. some in quantum optics, the decrease in efficiency for non-phasematched interactions is important to reduce the contribution of processes that interfere with the observation of the desired process. In these cases, careful consideration of the effects of both types of disorder in the domains is essential, as the $\mathrm{sinc}^2(x)$ roll-off will reach a disorder-limited floor [4].

3. Microstructured materials for QPM applications

Essential for a QPM interaction is a medium in which the nonlinear susceptibility can be patterned on a micron spatial scale, with long range order held to the strict tolerance described in Section 2.3. By far the best developed of these are periodically poled (PP) oxide ferroelectrics, but recent developments in orientation-patterned semiconductors and other microstructured media are opening a variety of other opportunities. In this section we describe essential features of these materials.

3.1. Ferroelectrics

3.1.1. Periodic poling

It was recognized as early as 1964 that multidomain ferroelectrics could enhance the efficiency of nonlinear interactions, due to the sign change in the nonlinear susceptibility accompanying domain reversal [5]. Efforts were made through periodic perturbation of crystal growth melts, and QPM interactions were demonstrated in periodically-poled (PP) media so produced, but adequate control of the long range order proved too difficult for widespread applications [6,7]. The first periodic poling methods under lithographic control were based on in-diffusion of a patterned dopant film [8], or ion exchange through a mask [9]. These methods produced domains that penetrated a depth in the substrate of order the domain period, enabling waveguide but not bulk interactions. Subsequently, electric-field poling methods, where the fields are applied to a periodic electrode pattern fabricated on the surface of the wafer, emerged [10], which can produce domains penetrating through millimeter-thick substrates, enabling both bulk and waveguide interactions. These electric-field methods have supplanted other poling methods for both types of interactions.

Electric-field poling methods for bulk crystals generally involve patterning a periodic electrode on one surface of the crystal, and applying voltage to produce a field exceeding the coercive field to reverse the domains in the electroded regions, Fig. 2. These methods rely on the steep dependence of the velocity of domain wall propagation on the electric field. As the domains propagate laterally beyond the electroded region, the uncompensated polarization charge slows the domain growth, ideally leading to self-termination of the process as the domain pattern approaches the desired duty cycle. A detailed discussion of the poling process can be found in Ref. [11]; Refs. [12] and [13] address other

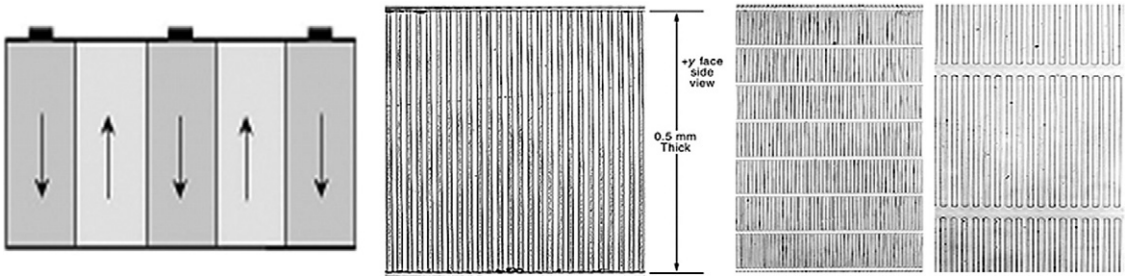

Fig. 2. (Left) Domain patterns expand underneath the electrode region when application of electric fields larger than the coercive field are used. (Center) These 15-μm-period domains propagate through 0.5-mm-thick substrates; aspect ratios greater than 100:1 are observed. (Right) Using photolithographic processes allows patterning of multi-grating devices. Here the +z surface of a 0.5-mm-thick PPLN chip is revealed by etching with hydrofluoric acid. Each grating is 500-μm wide and separated by 50 μm. The left panel shows a portion with periods 29–30.5 μm; the right panel shows a magnified view of the 29-μm period grating.

aspects of modeling of the domain patterning process. A large variety of poling processes have been developed to address the specific properties of various ferroelectrics [14,15].

3.1.2. Lithium niobate and tantalate

The first, and still the most widely exploited of the PP ferroelectrics are the lithium niobate ($LiNbO_3$, LN) and lithium tantalate ($LiTaO_3$, LT) family. Both are readily available in three- and four-inch diameter substrates, convenient for lithographic patterning and processing, and have established waveguide technologies compatible with periodic domain structures. The d_{33} coefficient in LN, 28 pm/V, is the largest among commonly used ferroelectrics, while that of LT is somewhat smaller, 16 pm/V. Both materials offer transparency into the near-UV, with absorption edges of 320 and 277 nm, for LN and LT, respectively, though both materials typically have absorption tails extending into the visible [16,17]. Quasi-phasematched SHG to wavelengths as short as 386 and 325 nm have been demonstrated in LN and LT [18,19]. In the mid-IR, multi-phonon absorption in both materials rises steeply in the range 4–5 μm, limiting high average power operation to wavelengths shorter than ∼4 μm, though CW interactions out to 6.6 μm, and short-pulse operation (enabling the use of short crystals) to wavelengths as long as 7.25 μm [20].

One serious issue for both these materials are photo-induced changes in the material properties, including both index changes (photorefractive effects) [21] and absorption changes (photochromic effects), e.g. green-induced infra-red absorption (GRIIRA) [22]. Photorefractive damage in these materials manifests itself as distortion of beams passing through the crystal, due to refractive index variations induced by the sequence of charge generation by photoionization of impurity levels in the gap, separation of the charges through a balance of the photogalvanic and ohmic currents, and the action of the resulting space charge field on the electrooptic tensor of the medium. It can be shown that these space charge fields are substantially reduced in periodically-poled compared to uniformly poled crystals [23], but for practical applications involving visible radiation, operation at elevated ($>100\,^{\circ}C$) temperatures is still generally required in the commonly available congruently melting compositions.

Materials resistant to photorefractive and photochromic effects are of practical importance. In recent years, use of both magnesium doping and compositions close to stoichiometric have been shown to be effective in this regard, in both cases apparently through reduction of the concentration of the anti-site Nb (Ta) defects present in large numbers in the congruent composition LN (LT). Czochralski-grown magnesium-doped, congruent LN [24], near-stoichiometric LT (SLT, produced both by double-crucible growth [25] and vapor-transport equilibration [26]), and lightly magnesium-doped near-stoichiometric LN [27] and LT [28] have all been successfully periodically-poled and are resistant to photorefractive and photochromic effects at room temperature.

Although the periodic poling of materials resistant to photorefractive and photochromic effects are still under investigation, efficient frequency conversion has been shown to cover the range from 460 nm to 2.8 microns in device lengths as long as 4 cm. In magnesium-doped, congruent LN, for example, periods as small as 1.4 microns have been achieved in devices suitable for bulk interactions. The large coercive fields of these materials have limited conventional poling to 1-mm-thick substrates and imposes a limit to the available aperture for high energy and peak power applications. Efforts to extend this thickness by diffusion bonding [29] and pulsed poling [30] techniques have increased usable thickness to 5 mm. Alternatively, periodic poling of rotated-cut substrates to enable QPM interactions

for beams incident on the surface rather than the edge of PP wafers may provide scalable apertures to the 4-inch-wafer scale [31].

3.1.3. KTP family

Potassium titanyl phosphate ($KTiOPO_4$, KTP) and its isomorphs are the other family of ferroelectrics that have been widely exploited for QPM applications. While typically available only in smaller wafers than the LN/LT family, and having a smaller d_{33} coefficient (17, 15, and 16 pm/V for KTP, $RbTiOPO_4$, and $KTiOAsO_4$, respectively) they offer the advantage of resistance to photorefractive damage at room temperature and higher surface damage thresholds [32].

Wavelengths as short as 359 nm have been generated by QPM SHG in PPKTP [33]. Multi-phonon absorption rises rapidly in the 3–4 μm range in KTP, so that the arsenate isomorphs, with multi-phonon absorption rising in the 4–5 μm range, are more useful for mid-IR applications. Wavelengths as long as 2.74 μm have been generated in PPKTP devices.

While the KTP family crystals are resistant to photorefractive damage, they are susceptible to "gray tracking", the development of long-lived color centers under intense visible radiation. Gray-tracking is a complex phenomenon, with complicated dependence on intensity, pulse repetition rate, spot size, and method of crystal growth [34].

Periodic poling of KTP has been shown to be possible to periods as short as 2.94 μm for lengths as long as 8 mm suitable for the generation of 390 nm light [35]. Due to the high ionic conductivity at room temperature, poling uniformity can improve when the periodic poling process occurs at low temperatures. This low temperature technique can provide periods of 4–39 μm over a length of 30 mm [15].

3.2. Semiconductors

Multiphonon absorption imposes a fundamental limit on the long-wavelength operation of QPM oxide ferroelectrics. The steep rise in absorption between 4 and 5 μm in $LiNbO_3$ and $LiTaO_3$, and between 3 and 4 μm in KTP make high average power operation difficult is this range. Alternative media with lower phonon energies offering transparency deeper into the mid-IR are therefore important for extending QPM techniques into the mid-IR.

The III–V and II–VI semiconductors have useful combinations of properties for mid-IR applications. GaAs, the best developed example, is transparent up to the weak three-phonon peak at ∼12 μm, has a large nonlinear susceptibility (95 pm/V, ∼4 times larger than that of $LiNbO_3$), and high thermal conductivity (52 W/m-K, ∼10 times larger than $LiNbO_3$). Early experiments in nonlinear optics addressed phasematching in these isotropic zincblende-structure crystals by assembly of QPM media from stacked plates polished to the coherence-length thicknesses [36,37]. The coherence lengths required for typical interactions are in the range of 10–100 μm [38]. These methods never found widespread use, due to difficulties in fabrication to the required tolerances, and the high losses associated with the many interfaces between the high-index plates and air. Elimination of these interfaces through diffusion bonding the stack into a single block by heating under pressure in a reducing atmosphere reduced the interface losses, but difficulties with fabrication to the required tolerances remained [39]. More recently, the phase shifts on total internal reflection in thin semiconductor plates have been explored as means to achieve QPM [40,41], again facing fabrication challenges.

A current method for microstructuring semiconductors for QPM is orientation-patterned growth. In these methods, a template substrate is patterned lithographically to create a pattern that controls the crystallographic orientation of subsequently grown films. Multilayer thin-film (microns) growth then produces a QPM waveguide; thick-film (∼ millimeter) growth produces a bulk QPM medium.

The concept of template-controlled growth for QPM applications was first demonstrated using ⟨100⟩/⟨111⟩-orientation effects in lattice-mismatched heteroepitaxial growth of CdTe and ZnTe films on GaAs substrates, but the propagation losses in ZnTe/ZnSe waveguides grown on these templates were too large for practical application [42]. A more successful method was based on diffusion bonding two [100] GaAs wafers, rotated 90° around [100] with respect to each other, on one of which there had previously been grown a thin GaAs film on an AlGaAs release layer. After etching away the release layer, a thin film with orientation rotated by 90° was left behind on the other wafer [43,44], which could then be lithographically patterned to form the orientation template. QPM devices in AlGaAs waveguides have been demonstrated based on this method.

The most widely used templates are now based on lattice-matched heteroepitaxy of GaAs/Ge films on GaAs substrates. Noting that interchanging the Ga and As atoms in a GaAs lattice results in the same structure as would a 90°

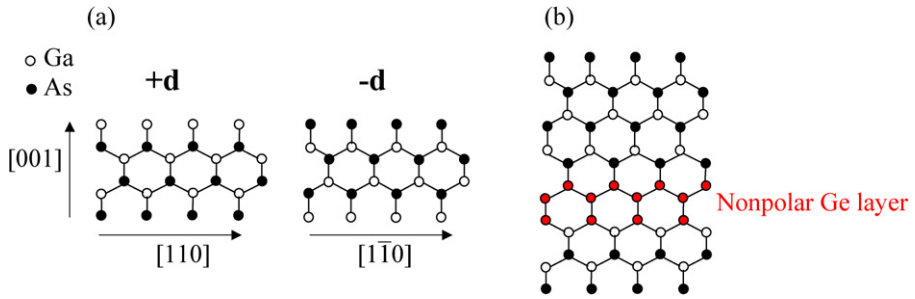

Fig. 3. (a) Atomic structure in GaAs and its inverted structure; (b) insertion of a nonpolar Ge layer allows growth of the inverted crystal above the original crystal.

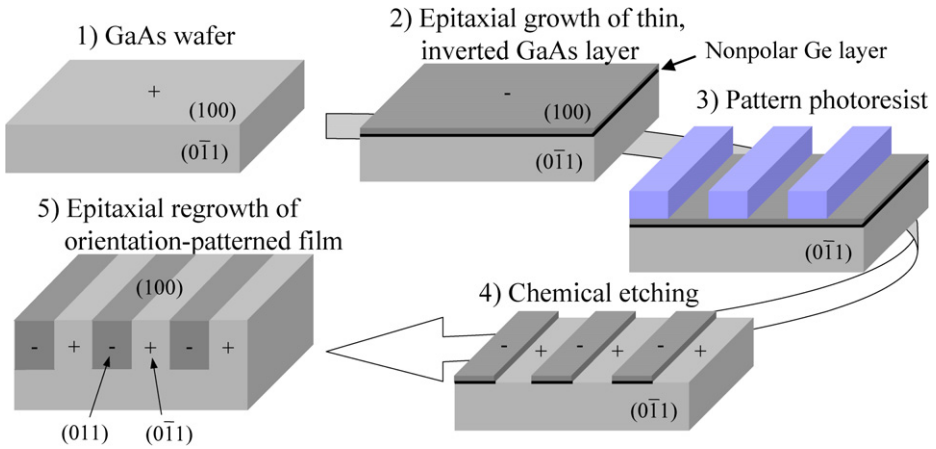

Fig. 4. Sketch of process flow for fabrication of an orientation-patterned GaAs template.

rotation of the original structure around [100] (see Fig. 3), and that Ga and As layers alternate along a [100] axis of GaAs, inserting a double layer of Ga (or As) would result in the crystal above the double layer being rotated 90° compared to that below the layer. While it is not possible to grow such a structure, growth of a thin Ge film, which is nonpolar and can accommodate subsequent growth initiated with either a Ga or an As layer, does allow the growth of a film whose orientation is rotated with respect to the substrate [45,46]. This is the essential step in the orientation-template process illustrated in Fig. 4. After lithographically patterning the rotated film to expose strips of the original substrate, subsequently grown films take the orientations of the underlying template regions. With thin-film growth, e.g. GaAs/AlGaAs, a QPM waveguide can be formed [47] (Section 4.3.2), while with thick film (typically hydride vapor-phase epitaxy, HVPE) growth, a bulk QPM medium is formed [48,49].

Details of the HVPE growth process for thick OP-GaAs films and its optimization are beyond the scope of this article. We confine ourselves to a sketch of the current capabilities and remaining challenges. Thick films of orientation-patterned GaAs (OP-GaAs) have been grown by both atmospheric-pressure [50] and low-pressure HVPE [48]. The latter enables much higher growth rates; up to ∼100 μm/h has been obtained, allowing growth of a 0.5-mm-thick film in only 5 hours. The thickest films grown in a single run have been ∼750-μm thick. With multiple growth runs, OP-GaAs films in excess of 1-mm thick have been produced, but the quality of the interface between the layers is not as high as in uniform regions. Domains with periods down to 40 μm have been grown reliably through 0.5-mm-thick films, and as short as 20 μm in 200-μm-thick films. Fig. 5 shows stain-etched cross sections of typical OP-GaAs films.

Template fabrication is not a limiting issue for thick film devices; details of the current process can be found in Ref. [51]. The growth of thick films on the templates remains a work in progress. Key issues for the growth include the fidelity of the domain pattern as it grows up through the film, the maximum thickness that can be grown before parasitic processes in the reactor limit the growth rate, the density of free carriers (which cause absorption in the mid-IR), and other sources of absorption and scatter loss. Free carrier absorption in the mid-IR is negligible, as

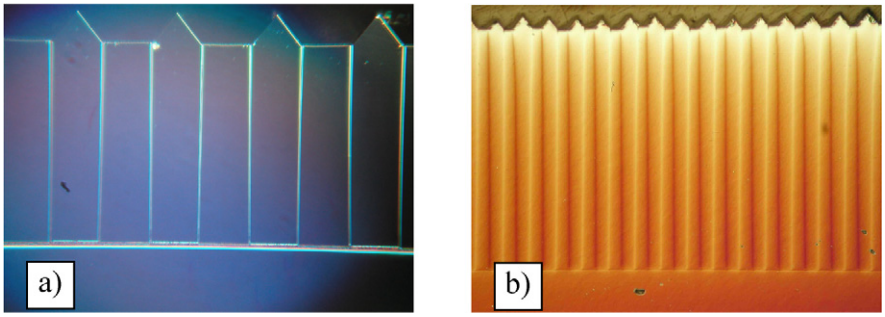

Fig. 5. Stain-etched cross-sections of OP-GaAs films with 80-μm period, where (a) is a short run that yielded a 220-mm thick film and demonstrates the characteristic "triangle-flat" free-surface shape, and (b) is a recent 700-mm-thick film with high domain fidelity.

densities of free carriers below $1 \cdot 10^{13}$ cm^{-3} are obtained. Extrinsic scatter and absorption losses remain a potential concern. Total losses in OP-GaAs of $\sim$0.01 cm^{-1} have been observed at 2-μm wavelengths.

3.3. QPM media for UV operation

While orientation patterned semiconductors offer a promising approach to the extension of QPM methods into the mid-IR and THz regimes, microstructured materials suitable for operation in the UV are less well developed. The deepest UV edge for oxide ferroelectrics currently in use is that of stoichiometric $LiTaO_3$, which is at $\sim$270 nm. Extrinsic absorption tails extending into the near-UV may limit practical operation to wavelengths longer than $\sim$350 nm, though QPM SHG has been demonstrated down to 325 nm [19]. Other media that have been investigated for UV operation include the fluoride ferroelectric $BaMgF_4$, and the ferrobielastic crystal quartz. Periodic domain patterns have been created in $BaMgF_4$ by electric-field poling, but have not yet been systematically exploited for QPM applications [52]. Ferrobielastics like quartz have orientation states that differ in their elastic compliance tensors, and hence have energies that differ in proportion to the square of applied stress fields, suggesting a switching process based on patterned stresses [53]. Periodically twinned quartz has been fabricated with a process using pressure applied to a plate with periodic surface relief, and has been used to demonstrate first-order QPM SHG of 532-nm radiation [54]. If the shorter pitch gratings required for UV operation are fabricated, the robustness and deep UV edge ($\sim$150 nm) of crystal quartz would make it a very attractive material for UV QPM.

4. QPM interactions

4.1. Theoretical background

In order to understand the scaling of QPM devices, it is useful to briefly review several aspects of conventional nonlinear device design.

4.1.1. Focused SHG

The plane-wave analysis given in Section 2.1 must be modified in order to describe SHG of focused Gaussian beams. The general theory is available in Ref. [55]. They cast the result in the form $P_{2\omega}/P_\omega = \eta_c L P_\omega$ where the focused efficiency, η_c, is given by

$$\eta_c = 16\pi^2 d_{\text{eff}}^2 h/\varepsilon_0 c n^2 \lambda^3 \tag{9}$$

where λ is the pump wavelength, n is the average refractive index, L is the length of the crystal, ε_0 is the permittivity of free space, and c the speed of light. h is the Boyd and Kleinman focusing parameter, taking the value 0.8 for confocal focusing and 1.1 for the optimum, tighter than confocal focus. Commonly, confocal focusing is used to reduce stress on the crystal. Because the area of the optimally focused beam increases linearly with the length of the medium, the efficiency scales only linearly rather than quadratically with the length of the medium. Similar considerations hold for focusing in other parametric conversion processes.

Including these focusing effects, QPM devices are seen to be very efficient for pump powers on the few watt scale. For example, SHG of 532 nm in LN, LT and KTP have normalized conversion efficiencies of 2.4%/(W-cm), 0.83%/(W-cm) and 1.7%/(W-cm) with confocal focusing conditions, so that in 5-cm-long samples the efficiencies are 12%/(W-cm), 4.2%/W, and 8.5%/W, respectively. The large nonlinear susceptibility of GaAs compensates for the decrease in efficiency associated with longer-wavelength interactions, e.g. for SHG of 2-μm radiation in OP-GaAs, the efficiency is 1.9%/(W-cm) compared to 0.38%/(W-cm) in PPLN.

4.1.2. Ultrafast SHG

In devices operating with ultrafast pulses, the additional consideration of the group velocity mismatch between the interacting waves must be considered. When the group delay difference through the length of the crystal becomes comparable to the duration of the pulses, the gain is significantly reduced below that calculated from quasi-stationary analysis [56]. Here, we summarize some simple conclusions for ultrafast SHG. The group velocity mismatch parameter, δv, is defined as

$$\delta v = 1/u_\omega - 1/u_{2\omega} \tag{10}$$

where $u_i = (\mathrm{d}\omega/\mathrm{d}k)|_{\omega_i}$ is the group velocity at the fundamental or second harmonic, and has typical values of several tenths of a picosecond per millimeter. The length over which a pump pulse will walk off the generated harmonic is $L_g = \tau/|\delta v|$, where τ is the pulse length. If we choose the length for the crystal to be $2L_g$, then for confocal focusing, it can be seen that the efficiency will scale only with the pulse energy. For transform-limited Gaussian pulses [56]

$$U_{2\omega}/U_\omega = \eta_{UF} U_\omega \tag{11}$$

where $U_{2\omega}$ and U_ω are the pulse energies at the fundamental and harmonic, respectively, and

$$\eta_{UF} = 76.7 d_{\mathrm{eff}}^2/\varepsilon_0 c n^2 \lambda_\omega^3 \delta v \tag{12}$$

For many materials there is a broad range of over which the efficiency is only weakly dependent on wavelength which is a result of the decrease as approximately λ^{-3} in group velocity mismatch compensating for the λ^{-3} scaling of the confocal SHG efficiency. Note that even though QPM interactions tend to have larger group velocity mismatch than BPM interactions (since they are not even phase velocity matched), the large nonlinear susceptibilities result in larger efficiencies for QPM than BPM interactions in most cases. The large group velocity mismatch can be used for pulse shaping functions, as discussed in Section 5.2.3.

Noncollinear interactions for group-velocity matching in QPM media have been analyzed in Refs. [57] and [58].

4.2. Bulk devices

It is not practical to comprehensively review the large body of device results based on QPM media. In this section, a few representative results are given indicating the range of performance available with QPM media used simply as highly nonlinear alternatives to conventional BPM media. Section 5 describes in more detail devices taking advantage of engineering freedom available only with QPM media.

QPM SHG has been demonstrated at wavelengths ranging from 325 nm in the UV [19] to 5.25 μm in the mid-IR [48]. Efficiencies close to those predicted theoretically have been observed in traveling wave SHG: up to 42% for CW 532-nm generation [59], 86% with ns pulses at 768 nm [60], and 52% with ps pulses [61]. Use of photorefractive- and photochromic-damage-resistant crystals has enabled high-average-power operation near room temperature, for example 5 W of 532-nm radiation was generated in PPSLT for 1000 h with no measurable degradation [26].

The high gain and low losses available in QPM media make them attractive for use in optical parametric oscillators (OPOs). An important early result was a 1.06-μm-pumped, CW, singly resonant, ring OPO in a 5-cm-long PPLN crystal, which had a threshold of 3.6 W and up to 95% pump depletion [62]. Tuning from 1.3–4.8 μm has been demonstrated in a 1.06-μm-pumped multigrating PPLN OPO [63], and 2.1–11 μm in an OP-GaAs OPO with a tunable ∼1.8-μm pump [64]. Reviews of early work in QPM OPOs can be found in Refs. [65] and [66].

The use of damage-resistant crystals has again proved useful for power scaling of OPOs and operation near room temperature. Over 60 W average power at 3.3 μm was generated in a 1.06-μm-pumped MgLN OPO at room

temperature [67]. Visible-wavelength pumping is enabled by current damage-resistant crystals, for example, a 532-nm-pumped near-stoichiometric lithium tantalate OPO generating 370 mW at 708 nm [68].

The high gains available in short crystal lengths make QPM media attractive for synchronously pumped OPOs. Pulses as short as 26 fs, [69] thresholds as low as 15 mW [70], and repetition rates up to 39 GHz [71] have been reported. Picosecond and femtosecond optical parametric generators have also been demonstrated in QPM media, with threshold pulse energies as low as 50 nJ with 0.5 ps pulses in PPLN, [72] and with greater than octave-wide continuum outputs in OP-GaAs (4.5–11 μm) [38].

QPM operation has been extended to THz spectral region in both ferroelectrics [73,74] and semiconductors [75].

4.3. Waveguide

4.3.1. Introduction

Early results in lithographically patterned QPM devices were of necessity obtained in waveguide geometries, because the diffusion-based poling processes then used led to domains that penetrated only several microns below the surface of the substrate [76–78]. The advent of electric-field poling methods lifted this constraint, but waveguide interactions remain important for some applications because they can have efficiencies several orders of magnitude larger than those in bulk media, a result of the waveguide confinement eliminating the tradeoff between a small spot size and a long interaction length.

The mathematical treatment of waveguide interactions is quite similar to that for plane waves, but with an effective area for relating the power to an effective intensity that depends on the overlap integral of the interacting waveguide modes [79]. The scaling of the mixing efficiency for undepleted-pump SHG then goes as

$$P_{2\omega}/P_{\omega} = \eta_0 L^2 P_{\omega} \tag{13}$$

where the normalized conversion efficiency $\eta_0[\%/\text{W-cm}^2]$ is proportional to the square of the nonlinear susceptibility and the modal overlap integral. Typical values for LN waveguides operating with a 1.5-μm pump are $\sim 100\%/(\text{W-cm}^2)$, so that a 6-cm-long device can have efficiencies of $>3000\%/\text{W}$. Operation with milliwatts of pump power is therefore possible, one of the attractive features of waveguide devices compared to bulk interactions. For typical waveguide designs, η_0 scales as λ^{-4}, with one factor of λ^{-2} from the inherent scaling of plane-wave SHG, and one factor of λ^{-2} from the increase in the effective area due to the increase in mode size with wavelength.

4.3.2. Waveguide fabrication

In QPM ferroelectrics, waveguide fabrication techniques compatible with domain patterning are required. The commonest approaches have involved diffusion of dopants, either at low temperatures after domain patterning, e.g. annealed proton exchange in PPLN [80], or at high temperatures prior to domain patterning, e.g. titanium diffusion in PPLN [81]. The diffusion of typical dopants into photorefractive-damage-resistant materials (Section 3.1.2) appears to increase their damage susceptibility [82], so techniques that evade this problem are of interest. Recently, ridge waveguides have been fabricated by bonding periodically-poled plates to a substrate, polishing the plate down to the desired waveguide thickness, and mechanically sawing the sidewalls of the ridge [83,84]. These waveguides appear capable of supporting visible powers in excess of 1 W.

Ion exchange, e.g. Rb or Ag, through a mask can provide both the high index segmented waveguide and the periodic domain inversion required for QPM in KTP [85–87]. Waveguides fabricated with these techniques are capable of generating 10s of milliwatts in the visible and can extend to a few milliwatts of ultraviolet radiation [33,88]. These fabrication methods also allow the integration of Bragg reflectors for resonant SHG and parametric oscillator devices [89].

In orientation-patterned semiconductors, growth of the waveguide structure proceeds at the same time as the patterned medium itself. Typically a low refractive index cladding, e.g. AlGaAs, is grown on the orientation template, followed by a higher refractive index core, e.g. GaAs, and perhaps an upper cladding layer. Ridge waveguides can then be etched in this structure. Both MOCVD [90] and MBE [47] have been used to grow orientation-patterned AlGaAs films. A key issue in this growth is control of the surface morphology to minimize losses [91].

4.3.3. Waveguide devices

Early work on waveguide QPM devices focused on generation of coherent radiation, especially conversion of IR semiconductor lasers to the visible and UV for optical data storage applications [78]. Work in this area decreased with

the advent of UV GaN diode lasers, but has recently revived for applications like displays requiring higher powers and longer (blue and green) wavelengths than are readily obtained in the InGaN system [92]. Recent results include reports of CW powers of 1.08 W in a single-mode PPMgLN planar waveguide with efficiency of 30% [93]. Tunable mid-IR radiation has also been generated at milliwatt power levels by difference frequency mixing in PPLN waveguides [94]. Low threshold optical parametric oscillation [95,96] and generation [97] have also been demonstrated.

More recently, applications to optical signal processing have been widely investigated. These applications can be viewed as optical domain analogues to RF mixers, where an output field is generated proportional to the product of two input fields, i.e. for difference frequency mixing, $E_{\text{out}} \propto E_p E_s^*$. A pump at frequency ω_p and a signal at ω_s produces an output at $\omega_{\text{out}} = \omega_p - \omega_s$. For near degenerate operation, with $\omega_p = 2\omega_s + \Delta$, the output is slightly shifted, to $\omega_{\text{out}} = \omega_s + \Delta$.

Thus, a pump close to ∼750 nm (or the second harmonic of a 1.5-μm pump) can shift 1.5-μm radiation within the C-band, and can be used for processing optical signals. With a CW pump, the optical carrier can be shifted while maintaining the amplitude, frequency and phase information of the envelope ("wavelength conversion"). The dependence of the output on the complex conjugate of the input can be used to compensate for chromatic dispersion in fiber links (mid-span spectral inversion). With a pulsed pump the mixing is gated, producing an output only when clock and data pulses are simultaneously present, an operation that can be used for multiplexing in the time domain. These optical signal processing functions in QPM waveguides are reviewed in Ref. [98].

Recently, generation and manipulation of single photons and photon pairs in QPM waveguides has been used for quantum optical signal processing, for example generating photon pairs by parametric down conversion [99], and efficient upconversion of 1.5-μm photons to ∼700 nm by sum frequency generation to enable photon counting with a silicon avalanche photodiode [100]. These applications are reviewed in Refs. [101] and [102].

5. Spatially inhomogeneous gratings

In addition to the applications described in Section 2, which demonstrate the utility of QPM media as high-performance alternatives to conventional BPM media, there are a number of effects that are unique to QPM media. These generally involve using transverse or longitudinal shaping of the QPM grating to engineer spatial or spectral responses different from those that can be obtained with simple periodic QPM gratings. We consider these two types of QPM engineering separately in the following two sections.

5.1. Transversely varying gratings

5.1.1. Multi-gratings and fan gratings

Varying the structure of a QPM grating normal to the direction of beam propagation can be used for a number of purposes. The most obvious of these is to make QPM devices tunable simply by translating the crystal so that the beam traverses different QPM structures. The simplest of these to fabricate is an array of gratings, each with a different QPM period, as shown in Fig. 3. In one demonstration, a crystal with 25 different gratings, ranging in period from 26 to 32 μm in 0.25 μm steps was used as the gain element in a 1.06-μm-pumped OPO to produce IR radiation tunable from 1.36- to 4.83-μm wavelengths, with interpolation between the steps with temperature tuning [63].

Fabrication of a fan-shaped grating allows continuous tuning of the QPM wavelength, though the limited fan angles compatible with fabrication of high-quality domain patterns limit the range accessible in a single chip. Continuous tuning of DFG and OPA with fan gratings has been demonstrated [103].

5.1.2. Angled gratings

Double-pass interactions and intracavity devices resonating all interacting waves can be used to increase the mixing efficiency over simpler designs, but at the cost of introducing sensitivity to the relative phases of the interacting waves. A variety of techniques have emerged to adjust this phase, which is typically difficult to set a priori due to the phase shifts on elements like the dielectric mirror coatings [104]. These techniques typically add the complexity, size, and/or loss of the device. A convenient, lossless approach that is possible in QPM media is to tilt the domain pattern at a small angle to the output facet of the crystal. Translation of the crystal normal to the beam propagation direction then changes the fraction of a coherence length in the last period of the crystal, allowing continuous adjustment of the relative phase of the interacting waves with no additional components in the cavity [105].

5.1.3. Radially varying grating strength

Reaching high efficiencies in traveling-wave interactions involving Gaussian beams in bulk media is difficult due to the intensity-dependent conversion, which leads to the center of the beam being driven towards depletion (and back-conversion) before the wings of the beam reach high conversion. This effect is exacerbated in pulsed interactions, where the peak in time is more strongly converted than the temporal wings of the pulse. In QPM media, it is possible to engineer gratings to partially overcome this difficulty.

Considering SHG for simplicity, the conversion efficiency for a phasematched plane wave interaction can be written as $\eta \equiv I_{2\omega}/I_\omega = \tanh^2(\sqrt{\eta_0})$, which depends only on the "drive" $\eta_0 \propto d_m^2 L^2 I_\omega$ [106]. For a weakly focused Gaussian pump beam of the form $I_\omega(r) = I_0 \exp(-2r^2/w_0^2)$, the conversion will vary radially with the local intensity in a uniformly patterned QPM grating. However, if the length of the grating is made to vary radially (by leaving a radially varying length of the medium unpoled) or the effective nonlinear coefficient is made to vary radially (by radially varying the duty cycle of the QPM grating), then the radial variation of the drive can be suppressed out to some radius. Experimental demonstration of this concept is shown in Ref. [106], out to radii of $0.75w_0$. Note that for a conventional z-cut crystal, patterning is not possible in the depth dimension, so that control over the drive is only possible in one spatial dimension (unless two crystals rotated 90° to each other are used). In face-pumped interactions in rotated-cut crystals (Section 3.1.2), two-dimensional patterning is possible.

5.1.4. Nonlinear physical optics

More complex transverse patterning of the QPM grating can be used to carry out nonlinear manipulations of wavefronts analogous to those familiar from conventional physical optics [107]. The simplest such "nonlinear physical optics" device is simply a single narrow strip of periodic-poling in a wide crystal. Illumination of this strip with a pump beam wider than the patterned region will create a harmonic wave only in the patterned region, effectively a "single-slit" source of the harmonic wave, with a top-hat near-field profile and a $\mathrm{sinc}^2(x)$ pattern in the far-field, just as in conventional single-slit diffraction. Such a slit source can serve as the building block of more complex functions, e.g. two such poled strips then serves as a double slit; the relative phase of the two slits can be controlled by the phase of the QPM gratings in the two strips. An array of poled strips with a quadratically varying phase across them serves as a Fresnel lens, and has been used to create diffraction-limited focusing of generated harmonic beams from a collimated input pump beam. An interesting feature if such "lenses" is that they form a converging beam in one direction and a diverging beam in the other [107].

5.2. Longitudinally varying gratings

5.2.1. Multi-grating interactions

A useful degree of design freedom in QPM media is the use of two or more gratings in sequence in the same crystal. These can be used, for example, to phasematch SHG in the first grating, and then sum the SH and fundamental to produce third harmonic in the second grating [108]. The reduced number of interfaces and simpler anti-reflection coating requirements in such arrangements are of particular value for intracavity applications, for example nonlinear outcoupling of an OPO by summing the resonant signal wave with the residual pump [109].

5.2.2. Fourier synthetic gratings

As seen in Section 2.2, the use of QPM with a uniform grating does not alter either the $\mathrm{sinc}^2(x)$ shape or the spectral bandwidth of the interaction. There are many situations where it is useful to alter the shape, the bandwidth, or both, to suit specific applications. Longitudinally-varying QPM gratings make it possible to systematically engineer both the spectral amplitude and phase of nonlinear mixing processes [110,111].

The basis for this spectral engineering is the dependence of the tuning behavior on the spatial Fourier transform of the nonlinear coefficient distribution, as can be seen in Eq. (2), the basic relation for the generated SH field. The transform variable, Δk, is usually a linear function of frequency, i.e.

$$\Delta k(\omega) \approx (\mathrm{d}k_{2\omega}/\mathrm{d}\omega - \mathrm{d}k_\omega/\mathrm{d}\omega)(\omega - \omega_0) = \delta v(\omega - \omega_0) \tag{14}$$

where ω_0 is a reference frequency for which it is assumed $\Delta k(\omega_0) = 0$, and we recall the definition of the inverse group velocity mismatch from Section 4.1.2, so the dependence of the conversion on frequency is just a scaled version of the dependence on Δk [112].

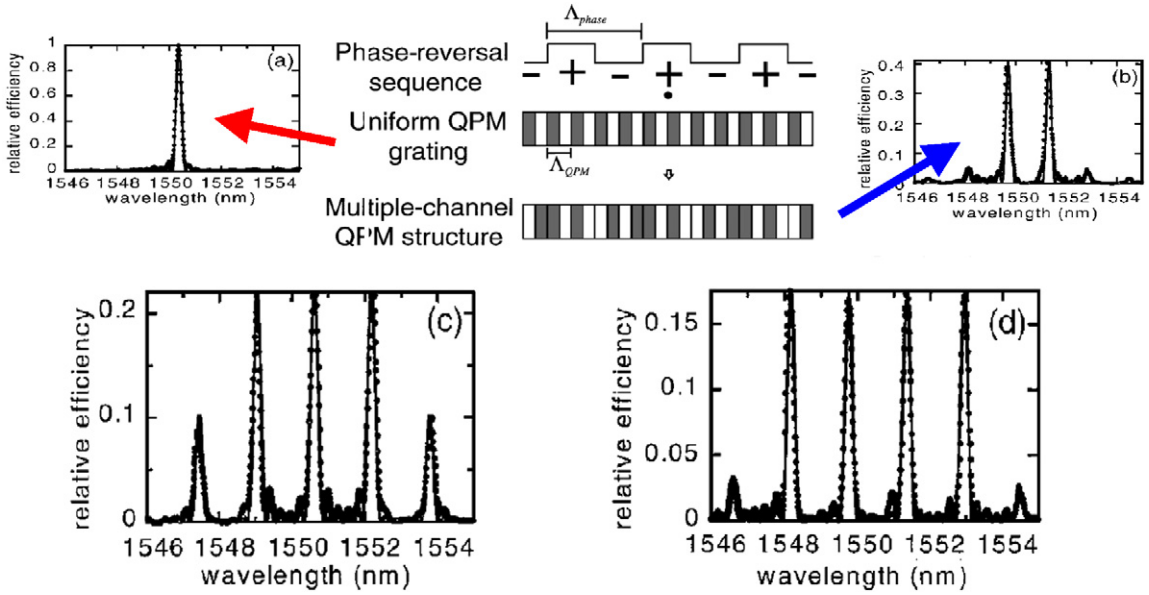

Fig. 6. Diagram depicting phase reversal in QPM devices. (a) A uniform grating produces a single sinc [2] peak. (b) A simple 50% duty cycle phase reversal sequence creates two QPM peaks. This technique can be generalized to produce (c) three-peak, and (d) four-peak devices. The filled circles are measured results, and the solid curves are theoretical fits. The efficiencies are relative to the peak efficiency (500%/W) of a single-peak device.

This identification is a powerful tool for understanding and designing tuning behavior of QPM gratings. For conventional phasematching, the nonlinear coefficient is simply a top-hat of length L, whose Fourier transform is just $\operatorname{sinc}(\Delta kL/2)$, corresponding to the familiar tuning behavior centered at $\Delta k = 0$. For QPM with a periodic grating, the nonlinear susceptibility is the product of a top-hat of length L and a function periodic in K_g, so by the Fourier shift theorem, the sinc function is unchanged, but shifted to center at $\Delta k = K_g$, another way to describe the familiar result for QPM in uniform grating.

More interesting results can be obtained by generalizing the same understanding to more complicated gratings. In general, choosing a QPM grating that is the inverse Fourier transform, appropriately scaled, of a desired spectral tuning function is a systematic way to obtain generalized tuning behaviors. For example, two QPM peaks can be obtained by choosing a grating function that is the product of two periodic functions, whose average spatial frequency sets the center of the pattern and the difference of whose spatial frequencies sets the splitting of the peaks. Experiments generalizing this concept to four peaks are shown in Fig. 6 [113].

Some general conclusions can be reached, independent of the details of the QPM pattern. From Parseval's theorem for Fourier transforms, it can be seen that the area under the square magnitude of the tuning curve is proportional to the length of the device, e.g. for a uniform grating the height goes as L^2 and the width as $1/L$, and that this area is unchanged by any "phase-only" pattern, i.e. one that maintains the local 50% duty-cycle of the grating. Thus, for example, in a grating designed to have N QPM peaks, the maximum of each of those peaks can be only $1/N$ that of the single peak of a uniform grating in a sample of the same length.

Various techniques have been developed to facilitate design of particular tuning behaviors under the constraint that only the sign, but not the magnitude of the teeth of the QPM grating can be set in ferroelectrics, and that there is generally a minimum feature size that can be reached conveniently [114–117]. Other techniques can be used to apodize the $\operatorname{sinc}^2(x)$ shape by engineering the average value of the QPM grating through phase reversal deletion or local duty cycle control [118]. Two-dimensional periodic patterning of the QPM grating creates an array of Fourier components that can be used to phasematch a sequence of noncollinear processes [119].

5.2.3. Chirped QPM gratings for ultrafast nonlinear optics

Among the most interesting applications of aperiodic QPM gratings are in the manipulation of ultrafast pulses. The physics underlying these effects can be seen in either the time or frequency domains, which are compared in Fig. 7. We consider SHG for simplicity, though similar concepts apply to other interactions.

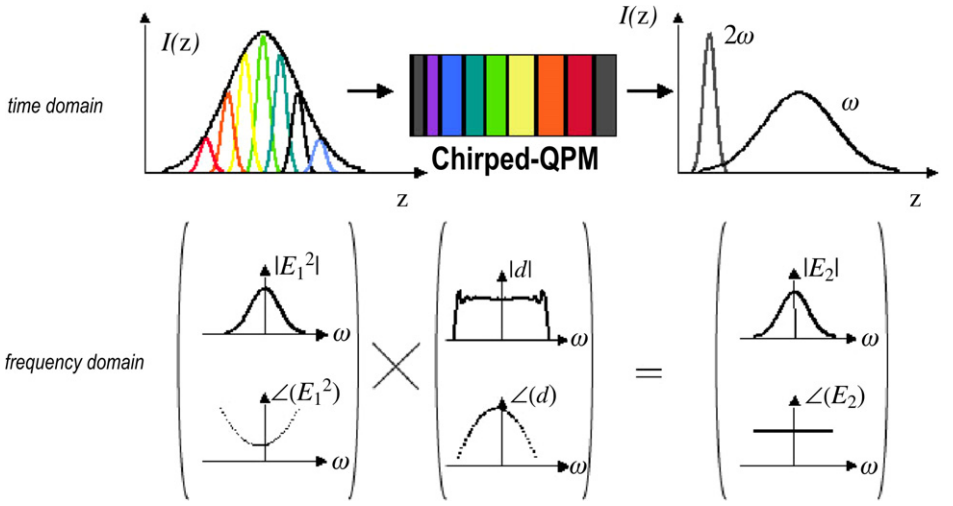

Fig. 7. Time- and frequency-domain interpretations of the effect of a chirped QPM grating on SHG of a chirped pulse. *Time domain*: Each spectral component of the pulse is quasi-phasematched in a different section of the grating. Those converted to the SH near the input of the crystal experience a longer group delay than those converted to SH near the output, because the group velocity of the SH is smaller than that of the fundamental. *Frequency domain*: The effect of the QPM conversion can be viewed as a transfer function from the spectrum of the square of the pump field to the spectrum of the SH field. The transfer function depends on the Fourier transform of the grating, and for a linear chirp has a parabolic phase and flat amplitude. The output SH pulse is transform limited if the phase of the transfer function is equal and opposite to that of the input pulse.

Consider first a time domain description, for the case of a short pulse being converted to the SH in a linearly chirped QPM grating, i.e. one in which the k-vector of the QPM grating is $K_g(z) = K_0 + K'z$. The two key points are that (1) a given spectral component of pulse will be phasematched only in a small region around the point where the grating vector is appropriate for QPM of that wavelength, and (2) as discussed in Section 4.1.2, the fundamental and the harmonic move with different group velocities in the dispersive crystal. Spectral components converted near the input of the crystal and hence propagating at the slower SH group velocity along most of the length of the medium emerge with a long group delay compared to those components that convert near the output of the crystal, and hence propagated at the fundamental group velocity through most of the length. By choosing the chirp rate of the QPM grating, and hence the location where different spectral components of the pulse are phasematched, a nearly arbitrary wavelength dependent group delay can be programmed into the crystal. The maximum group delay difference available is simply $L\delta v$, where δv is the difference in inverse group velocities defined in Section 4.1.2, and the QPM bandwidth $\Delta\omega$ is simply given by the wavelengths phasematched by $K_g(0)$ and $K_g(L)$. As an example, for SHG of a 1.5-μm pump in PPLN, $\delta v = 0.35$ ps/mm so that ∼17 ps group delay difference is available in a 50-mm-long crystal. Due to the dispersion of PPLN (and most other materials) the available group delay scales approximately as λ^{-3}. So that considerably longer delays are available at shorter wavelengths.

As a simple example of the use of such a linearly chirped grating, if the group delay spectrum of the QPM grating is chosen to be equal and opposite to that on a chirped pump pulse, a compressed SH pulse can be generated. With a more general chirp function, a nearly arbitrary group delay spectrum can be generated, within the limits imposed by the maximum group delay difference given the available length of crystal.

A complementary picture of the action of chirped QPM gratings on ultrafast pulses can be obtained in the Fourier domain. From the arguments in Section 5.2.2, the spectral amplitude and phase of the conversion process depend on the Fourier transform of the QPM grating function. In the low conversion limit, where the spectrum $E_\omega(\Omega) = \widehat{E_\omega(t)}$ of the pump pulse can be viewed as unchanged in the conversion process, the QPM tuning curve can be viewed as a transfer function [120] filtering the spectrum $\widehat{E(t)^2}$ to generate the output SH spectrum, where $\widehat{f(t)}$ is the Fourier transform of $f(t)$ [121]. For a linearly chirped grating, the Fourier transform can be expressed in terms of Fresnel integrals, and for adequately strong chirps, the transfer function has a largely flat amplitude over the range $\Delta\omega$ of phasematched wavelengths, and has quadratic spectral phase (corresponding to the linear group delay vs frequency found in the time domain discussion in Section 4.1.2). If $\Delta\omega$ exceeds the bandwidth of the pump pulse, and the quadratic phase of the transfer function is equal and opposite in sign to that of the input pulse, a compressed output

SH pulse results. Again, a grating with a more general chirp function results in a transfer function with more general frequency dependence of the spectral phase [122].

These effects have been demonstrated experimentally in pulse compression during SHG [123], synthesis of various pulse trains from Gaussian input pulses in SHG [112] and DFG [124], compensation of cubic phase [122] and generation by SHG of synchronous two-color pulses with spectral brightness higher than that of the input pulse [125]. Transfer functions with tunable quadratic spectral phase were demonstrated using a grating with transversely varying chirp rate [126]. Blue pulses as short as 6 fs have been generated by SHG in a suitably chirped PPLT crystal [127].

The analysis of chirped QPM gratings in optical parametric amplifiers (OPAs) and OPOs is also mathematically tractable, but different from that of processes like SHG, DFG, and SFG, and does not yield a simple Fourier transform relationship for the transfer function. Simple expressions are available in useful limits [128], and the time domain arguments for understanding the spectral phase from the localized conversion around the phasematched point, and the difference in group velocities (in this case between the signal and idler waves) can still be applied. Experimental demonstrations of OPA [129] and OPO [130] bear out these concepts. Tandem crystal designs have been developed for OPAs with flat amplitude and group delay across octave bandwidths [131].

6. Summary and future directions

Quasi-phasematched nonlinear interactions in microstructured ferroelectrics and semiconductors have developed over the past twenty years into an important method for the generation of coherent radiation, and for classical and quantum optical signal processing. QPM interactions offer both operation analogous to conventionally phasematched interactions, but with higher nonlinear mixing efficiencies, and functionalities unavailable with conventional phasematching. The materials available for QPM have expanded to include photorefractive damage resistant ferroelectrics allowing room temperature operation with high optical powers, orientation-patterned semiconductors extending QPM techniques to the mid-IR, and waveguides enabling efficient interactions with milliwatt optical powers. Techniques have emerged for engineering spatial and spectral properties of nonlinear interactions through the use of aperiodic QPM gratings.

Opportunities for future work in QPM nonlinear optics exist in a number of areas. Further development of microstructured media suitable for UV operation like periodically twinned quartz or fluoride ferroelectrics would open that spectral range for QPM interactions. The orientation-patterned semiconductors are at an early stage of development; extension to wider bandgap materials such as GaP or ZnSe would enable near-IR-pumped interactions; fabrication of low-loss waveguides would open the mid-IR to efficient low-power interactions. Large aperture QPM media, like face-poled rotated-cut ferroelectrics, will enable devices using very high energy pulses such as chirped-pulse parametric amplifiers. The rich opportunities for engineering of spatial and spectral properties of nonlinear converters with aperiodic QPM gratings are barely tapped, e.g. exploitation in engineering OPAs with desirable gain and group delay spectra are only in the earliest stages. The development of damage-resistant and low-loss waveguides is opening opportunities both in integrated high-power sources, and signal processing in the classical and quantum domains.

References

[1] J.A. Armstrong, N. Bloembergen, J. Ducuing, P.S. Pershan, Interactions between light waves in a nonlinear dielectric, Phys. Rev. 127 (1962) 1918–1939.
[2] P.A. Franken, J.F. Ward, Optical harmonics and nonlinear phenomena, Rev. Mod. Phys. 35 (1963) 23–39.
[3] M.M. Fejer, G.A. Magel, D.H. Jundt, R.L. Byer, Quasi-phase-matched second harmonic generation: Tuning and tolerances, IEEE J. Quantum. Electron. QE-28 (1992) 2631–2654.
[4] L. Yunchu, Q. Wang, X. Zhang, D. Yuan, Z. Liu, Z. Jiang, Z. Liu, S. Li, S. Fan, S. Zhang, Influence of stochastic deviations of domain boundary and varying effective index on difference frequency mixing in quasi-phase-matching waveguides, Opt. Commun. 247 (2005) 205–212.
[5] R.C. Miller, Optical harmonic generation in single crystal $BaTiO_3$, Phys. Rev. 134 (1964) A1313–A1319.
[6] Y.H. Xue, N.B. Ming, J.S. Zhu, D. Feng, The second harmonic generation in $LiNbO_3$ crystals with period laminar ferroelectric domains, Chinese Phys. 4 (1984) 554–564.
[7] A. Feisst, P. Koidl, Current induced periodic ferroelectric domain structures in $LiNbO_3$, applied for efficient nonlinear optical frequency mixing, Appl. Phys. Lett. 47 (1985) 1125–1127.
[8] E.J. Lim, M.M. Fejer, R.L. Byer, Second harmonic generation of green light in a periodically-poled planar lithium niobate waveguide, Electron. Lett. 25 (1989) 174–175.

[9] C.J. van der Poel, J.D. Bierlein, J.B. Brown, S. Colak, Efficient type I blue second-harmonic generation in periodically segmented $KTiOPO_4$ waveguides, Appl. Phys. Lett. 57 (1990) 2074–2076.
[10] S. Matsumoto, E.J. Lim, H.M. Hertz, M.M. Fejer, Quasiphase-matched second harmonic generation of blue light in a electrically periodically-poled lithium tantalate, Electron. Lett. 27 (1991) 2040–2041.
[11] G.D. Miller, Periodically poled lithium niobate: modeling, fabrication, and nonlinear-optical performance, Ph.D. Thesis, Stanford University, Stanford, California, 1998, http://wwwlib.umi.com/cr/stanford/fullcit?p9901557.
[12] V.Y. Shur, E.L. Rumyantsev, E.V. Nikolaeva, E.I. Shishkin, R.G. Batchko, M.M. Fejer, R.L. Byer, I. Mnushkina, Domain kinetics in congruent and stoichiometric lithium niobate, Ferroelectrics 269 (2002) 1037–1042.
[13] P. Urenski, G. Rosenman, M. Molotskii, Fine mechanisms of polarization switching in $KTiOPO_4$ ferroelectric crystals, Ferroelectrics 268 (2002) 497–502.
[14] H. Ishizuki, I. Shoji, T. Taira, Periodical poling characteristics of congruent MgO:$LiNbO_3$ crystals at elevated temperature, Appl. Phys. Lett. 82 (2003) 4062–4064.
[15] G. Rosenman, A. Skliar, D. Eger, M. Oron, M. Katz, Low temperature periodic electrical poling of flux-grown $KTiOPO_4$ and isomorphic crystals, Appl. Phys. Lett. 73 (1998) 3650–3652.
[16] L. Kovacs, G. Ruschhaupt, K. Polgar, G. Corradi, M. Wohlecke, Composition dependence of the ultraviolet absorption edge in lithium niobate, Appl. Phys. Lett. 70 (1997) 2801–2803.
[17] C. Baumer, C. David, A. Tunyagi, K. Betzler, H. Hesse, E. Kratzig, M. Wohlecke, Composition dependence of the ultraviolet absorption edge in lithium tantalate, J. Appl. Phys. 93 (2003) 3102–3104.
[18] R. White, I. McKinnie, S. Butterworth, G. Baxter, D. Warrington, P. Smith, G. Ross, D. Hanna, Tunable single-frequency ultraviolet generation from a continuous-wave Ti:sapphire laser with an intracavity PPLN frequency doubler, Appl. Phys. B: Lasers and Optics 77 (2003) 547–550.
[19] J.P. Meyn, M.M. Fejer, Tunable ultraviolet radiation by second-harmonic generation in periodically poled lithium tantalate, Opt. Lett. 22 (1997) 1214–1216.
[20] M.A. Watson, M.V. O'Connor, P.S. Lloyd, D.P. Shepherd, D.C. Hanna, C.B.E. Gawith, L. Ming, P.G.R. Smith, O. Balachninaite, Extended operation of synchronously pumped optical parametric oscillators to longer idler wavelengths, Opt. Lett. 27 (2002) 2106–2108.
[21] F. Jermann, M. Simon, E. Kratzig, Photorefractive properties of congruent and stoichiometric lithium niobate at high light intensities, J. Opt. Soc. Am. B 12 (1995) 2066–2070.
[22] Y. Furukawa, K. Kitamura, A. Alexandrovski, R.K. Route, M.M. Fejer, G. Foulon, Green-induced infrared absorption in MgO-doped $LiNbO_3$, Appl. Phys. Lett. 78 (2001) 1970–1972.
[23] M. Taya, M.C. Bashaw, M.M. Fejer, Photorefractive effects in periodically poled ferroelectrics, Opt. Lett. 21 (1999) 857–859.
[24] D.A. Bryan, R. Gerson, H.E. Tomaschke, Increased optical damage resistance in lithium niobate, Appl. Phys. Lett. 44 (1984) 847–849.
[25] Y. Furukawa, K. Kitamura, E. Suzuki, K. Niwa, Stoichiometric $LiTaO_3$ single crystal growth by double crucible Czochralski method using automatic powder supply system, J. Crystal Growth 197 (1999) 889–895.
[26] M. Katz, R.K. Route, D.S. Hum, K.R. Parameswaran, G.D. Miller, M.M. Fejer, Vapor-transport equilibrated near-stoichiometric lithium tantalate for frequency-conversion applications, Opt. Lett. 29 (2004) 1775–1777.
[27] Y. Furukawa, K. Kitamura, S. Takekawa, K. Niwa, H. Hatano, Stoichiometric Mg:$LiNbO_3$ as an effective material for nonlinear optics, Opt. Lett. 23 (1998) 1892–1894.
[28] F. Nitanda, Y. Furukawa, S. Makio, M. Sato, K. Ito, Increased optical damage resistance and transparency in MgO-doped $LiTaO_3$ single crystals, Jpn. J. Appl. Phys. 34 (1995) 1546–1549.
[29] K. Nakamura, T. Hatanaka, H. Ito, High output energy quasi-phase-matched optical parametric oscillators using diffusion-bonded periodically poled and single domain $LiNbO_3$, Jpn. J. Appl. Phys. 40 (2001) L337–L339.
[30] H. Ishizuki, T. Taira, High-energy quasi-phase-matched optical parametric oscillation in a periodically poled MgO:$LiNbO_3$ device with a 5 mm × 5 mm aperture, Opt. Lett. 30 (2005) 2918–2920.
[31] D.S. Hum, R.K. Route, G.D. Miller, M.M. Fejer, Quasi-phase-matched second harmonic generation using 42° rotated Y-cut near-stoichiometric lithium tantalate, in: Conf. on Lasers and Electro-Optics, 2004, CthU2.
[32] M. Peltz, U. Bader, A. Borsutzky, R. Wallenstein, J. Hellstrom, H. Karlsson, V. Pasiskevicius, F. Laurell, Optical parametric oscillators for high pulse energy and high average power operation based on large aperture periodically poled KTP and RTA, Appl. Phys. B: Lasers and Optics 73 (2001) 663–670.
[33] F. Laurell, J.B. Brown, J.D. Bierlein, Simultaneous generation of UV and visible light in segmented KTP waveguides, Appl. Phys. Lett. 62 (1993) 1872–1874.
[34] B. Boulanger, I. Rousseau, J.P. Feve, M. Maglione, B. Menaert, G. Marnier, Optical studies of laser-induced gray-tracking in KTP, IEEE J. Quant. Electron. 35 (1999) 281–286.
[35] S. Wang, V. Pasiskevicius, F. Laurell, H. Karlsson, Ultraviolet generation by first-order frequency doubling in periodically poled $KTiOPO_4$, Opt. Lett. 23 (1998) 1883–1885.
[36] A. Szilagyi, A. Hordvik, H. Schlossberg, A quasi-phase matching technique for efficient optical mixing and frequency doubling, J. Appl. Phys. 47 (1976) 2025–2032.
[37] D.E. Thompson, J.D. McMullen, D.B. Anderson, Second harmonic generation in GaAs 'stack of plates' using high-power CO_2 laser radiation, Appl. Phys. Lett. 29 (1976) 113–115.
[38] P.S. Kuo, K.L. Vodopyanov, M.M. Fejer, D.M. Simanovskii, X. Yu, J.S. Harris, D. Bliss, D. Weyburne, Optical parametric generation of a mid-infrared continuum in orientation-patterned GaAs, Opt. Lett. 31 (2006) 71–73.
[39] D. Zheng, L.A. Gordon, Y.S. Wu, R.S. Feigelson, M.M. Fejer, R.L. Byer, K.L. Vodopyanov, 16-μm infrared generation by difference-frequency mixing in diffusion-bonded-stacked GaAs, Opt. Lett. 23 (1998) 1010–1012.

[40] R. Haidar, Ph. Kupecek, E. Rosencher, Nonresonant quasi-phase matching in GaAs plates by Fresnel birefringence, Appl. Phys. Lett. 83 (2003) 1506–1508.
[41] H. Komine, W.H. Long Jr., J.W. Tully, E.A. Stappaerts, Quasi-phase-matched second-harmonic generation by use of a total-internal-reflection phase shift in gallium arsenide and zinc selenide plates, Opt. Lett. 23 (1998) 661–663.
[42] M.J. Angell, R.M. Emerson, J.L. Hoyt, J.F. Gibbons, L.A. Eyres, M.L. Bortz, M.M. Fejer, Growth of alternating ⟨100⟩/⟨111⟩-oriented II–VI regions for quasi-phasematched nonlinear optical devices on GaAs substrates, Appl. Phys. Lett. 64 (1994) 3107–3109.
[43] L.A. Eyres, C.B. Ebert, P.J. Tourreau, J.S. Harris, M.M. Fejer, Demonstration of second harmonic generation in all-epitaxially grown orientation-patterned AlGaAs waveguides, in: Advanced Solid-State Lasers, OSA TOPS, 1999, pp. 689–694.
[44] S.J.B. Yoo, C. Caneau, R. Bhat, M.A. Koza, A. Rajhel, N. Antoniades, Wavelength con-version by difference frequency generation in AlGaAs waveguides with periodic domain inversion achieved by wafer bonding, Appl. Phys. Lett. 68 (1996) 2609–2611.
[45] S.J. Koh, T. Kondo, T. Ishiwada, C. Iwamoto, H. Ichinose, H. Yaguchi, T. Usami, Y. Shiraki, R. Ito, Sublattice reversal in GaAs/Si/GaAs(100) heterostructures by molecular beam epitaxy, Jpn. J. Appl. Phys. 37 (1998) L1493–L1496.
[46] C.B. Ebert, L.A. Eyres, M.M. Fejer, J.S. Harris, MBE growth of antiphase GaAs films using GaAs/Ge/GaAs heteroepitaxy, J. Crystal Growth 201/202 (1999) 187–193.
[47] X. Yu, L. Scaccabarozzi, J.S. Harris, P.S. Kuo, M.M. Fejer, Efficient continuous wave second harmonic generation pumped at 1.55 μm in quasi-phase-matched AlGaAs waveguides, Opt. Express 13 (2005) 10742–10753.
[48] L.A. Eyres, P.J. Tourreau, T.J. Pinguet, C.B. Ebert, J.S. Harris, M.M. Fejer, L. Becouarn, B. Gerard, E. Lallier, All-epitaxial fabrication of thick, orientation-patterned GaAs films for nonlinear optical frequency conversion, Appl. Phys. Lett. 79 (2001) 904–906.
[49] D.F. Bliss, C. Lynch, D. Weyburne, K. O'Hearn, J.S. Bailey, Epitaxial growth of thick GaAs on orientation-patterned wafers for nonlinear optical applications, J. Crystal Growth 287 (2006) 673–678.
[50] L. Becouarn, B. Gerard, M. Brevignon, J. Lehoux, Y. Gourdel, E. Lallier, Second harmonic generation of CO_2 laser using thick quasi-phase-matched GaAs layer grown by hydride vapour phase epitaxy, Electron. Lett. 34 (1998) 2409–2410.
[51] X. Yu, MBE growth of III–V materials with orientation-patterned structures for nonlinear optics, Ph.D. Thesis, Stanford University, Stanford, California, 2006, http://wwwlib.umi.com/cr/stanford/fullcit?p3209028.
[52] S.C. Buchter, T.Y. Fan, V. Liberman, J.J. Zayhowski, M. Rothschild, E.J. Mason, A. Cassanho, H.P. Jenssen, J.H. Burnett, Periodically poled $BaMgF_4$ for ultraviolet frequency generation, Opt. Lett. 26 (2001) 1693–1695.
[53] S. Kurimura, N.E. Yu, K. Kitamura, T. Yamada, K. Hayashi, Periodical twinning for quasiphase-matched quartz, in: Conf. on Lasers and Electro-Optics, 2003, CMF3.
[54] T. Yamada, K. Hayashi, S. Kurimura, N.E. Yu, K. Kitamura, Harmonic generation characteristics of QPM quartz in visible-to-UV region, in: Quant. Electron. and Laser Science Conf., 2005, JtuC38.
[55] G.D. Boyd, D.A. Kleinman, Parametric interaction of focused Gaussian light beams, J. Appl. Phys. 39 (1968) 3597–3639.
[56] G. Imeshev, M.A. Arbore, M.M. Fejer, A. Galvanauskas, M. Fermann, D. Harter, Ultrashort-pulse second-harmonic generation with longitudinally nonuniform quasi-phase-matching gratings: pulse compression and shaping, J. Opt. Soc. Am. B 17 (2000) 304–318.
[57] S. Ashihara, T. Shimura, K. Kuroda, Group-velocity matched second-harmonic generation in tilted quasi-phasematched gratings, J. Opt. Soc. Am. B 20 (2003) 853–856.
[58] A.M. Schober, M. Charbonneau-Lefort, M.M. Fejer, Broadband quasi-phase-matched second-harmonic generation of ultrashort optical pulses with spectral angular dispersion, J. Opt. Soc. Am. B 22 (2005) 1699–1713.
[59] G.D. Miller, R.G. Batchko, W.M. Tulloch, D.R. Weise, M.M. Fejer, R.L. Byer, 42%-efficient single-pass CW second-harmonic generation in periodically poled lithium niobate, Opt. Lett. 22 (1997) 1834–1836.
[60] D. Taverner, P. Britton, P.G.R. Smith, D.J. Richardson, G.W. Ross, D.C. Hanna, Highly efficient second-harmonic and sum-frequency generation of nanosecond pulses in a cascaded erbium-doped fiber: periodically poled lithium niobate source, Opt. Lett. 23 (1998) 162–164.
[61] V. Pruneri, S.D. Butterworth, D.C. Hanna, Highly efficient green-light generation by quasi-phase-matched frequency doubling of picosecond pulses from an amplified mode-locked Nd:YLF laser, Opt. Lett. 21 (1996) 390–392.
[62] W.R. Bosenberg, A. Drobshoff, J.I. Alexander, L.E. Myers, R.L. Byer, 93% pump depletion, 3.5-W continuous-wave, singly resonant optical parametric oscillator, Opt. Lett. 21 (1996) 1336–1338.
[63] L.E. Myers, R.C. Eckardt, M.M. Fejer, R.L. Byer, W.R. Bosenberg, Multigrating quasi-phase-matched optical parametric oscillator in periodically poled $LiNbO_3$, Opt. Lett. 21 (1996) 591–593.
[64] K.L. Vodopyanov, O. Levi, P.S. Kuo, T.J. Pinguet, J.S. Harris, M.M. Fejer, B. Gerard, L. Becouarn, E. Lallier, Optical parametric oscillation in quasi-phase-matched GaAs, Opt. Lett. 29 (2004) 1912–1914.
[65] L.E. Myers, R.C. Eckardt, M.M. Fejer, R.L. Byer, W.R. Bosenberg, J.W. Pierce, Quasi-phasematched optical parametric oscillators using bulk periodically poled $LiNbO_3$, J. Opt. Soc. Am. B 12 (1995) 2102–2116.
[66] L.E. Myers, W.R. Bosenberg, Periodically poled lithium niobate and quasi-phase-matched optical parametric oscillators, IEEE J. Quant. Electron. 33 (1997) 1663–1672.
[67] Y. Hirano, S. Yamamoto, T. Tajime, H. Taniguchi, M. Nakamura, High-power, room-temperature operation of a PPMgLN OPO, in: Conf. on Lasers and Electro-Optics, 2000, Post-Deadline 7, pp. 13–14.
[68] S.-Y. Tu, A.H. Kung, Z.D. Gao, S.N. Zhu, Efficient periodically poled stoichiometric lithium tantalate optical parametric oscillator for the visible to near-infrared region, Opt. Lett. 30 (2005) 2451–2453.
[69] J. Hebling, X.P. Zhang, H. Giessen, J. Kuhl, J. Seres, Pulse characteristics of an optical parametric oscillator pumped by sub-30-fs light pulses, Opt. Lett. 25 (2000) 1055–1057.
[70] K.A. Tillman, D.T. Reid, D. Artigas, J. Hellstrm, V. Pasiskevicius, F. Laurell, Low-threshold femtosecond optical parametric oscillator based on chirped-pulse frequency conversion, Opt. Lett. 28 (2003) 543–545.
[71] S. Lecomte, R. Paschotta, S. Pawlik, B. Schmidt, K. Furusawa, A. Malinowski, D.J. Richardson, U. Keller, Optical parametric oscillator with a pulse repetition rate of 39 GHz and 2.1-W signal average output power in the spectral region near 1.5 μm, Opt. Lett. 30 (2005) 290–292.

[72] A. Galvanauskas, M.A. Arbore, M.M. Fejer, M.E. Fermann, D. Harter, Fiber-laser-based femtosecond parametric generator in bulk periodically poled $LiNbO_3$, Opt. Lett. 22 (1997) 105–107.
[73] Y. Sasaki, A. Yuri, K. Kawase, H. Ito, Terahertz-wave surface-emitted difference frequency generation in slant-stripe-type periodically poled $LiNbO_3$ crystal, Appl. Phys. Lett. 81 (2002) 3323–3325.
[74] Y.-S. Lee, T.B. Norris, Terahertz pulse shaping and optimal waveform generation in poled ferroelectric crystals, J. Opt. Soc. Am. B 19 (2002) 2791–2794.
[75] K.L. Vodopyanov, M.M. Fejer, D.M. Simanovskii, V.G. Kozlov, Y.-S. Lee, Terahertz-wave generation in periodically-inverted GaAs, in: Conf. on Lasers and Electro-Optics 2005, pp. 1450–1452.
[76] E.J. Lim, M.M. Fejer, R.L. Byer, W.J. Kozlovsky, Blue light generation by frequency doubling in a periodically poled lithium niobate channel waveguide, Electron. Lett. 25 (1989) 731–732.
[77] K. Yamamoto, K. Mizuuchi, T. Taniuchi, Milliwatt-order blue-light generation in a periodically domain-inverted $LiTaO_3$ waveguide, Opt. Lett. 16 (1991) 1156–1158.
[78] M.M. Fejer, Nonlinear frequency conversion in periodically-poled ferroelectric waveguides, in: D.B. Ostrowsky, R. Reinisch (Eds.), Guided Wave Nonlinear Optics, Kluwer Academic Publishers, Dordrecht, 1992, pp. 133–145.
[79] M.L. Bortz, S.J. Field, M.M. Fejer, D. Nam, R. Waarts, D. Welch, Noncritical quasi-phasematched second harmonic generation in an annealed proton-exchanged $LiNbO_3$ waveguide, IEEE J. Quant. Electron. 30 (1994) 2953–2960.
[80] K.R. Parameswaran, R.K. Route, J.R. Kurz, R.V. Roussev, M.M. Fejer, M. Fujimura, Highly efficient second-harmonic generation in buried waveguides formed by annealed and reverse proton exchange in periodically poled lithium niobate, Opt. Lett. 27 (2002) 179–181.
[81] G. Schreiber, H. Suche, Y.L. Lee, W. Grundkötter, V. Quiring, R. Ricken, W. Sohler, Efficient cascaded difference frequency conversion in periodically poled Ti:$LiNbO_3$ waveguides using pulsed and cw pumping, Appl. Phys. B: Lasers and Optics 73 (2001) 501–504.
[82] M. Asobe, O. Tadanaga, T. Yanagawa, H. Itoh, H. Suzuki, Reducing photorefractive effect in periodically poled ZnO- and MgO-doped $LiNbO_3$ wavelength converters, Appl. Phys. Lett. 78 (2001) 3163–3165.
[83] K. Mizuuchi, T. Sugita, K. Yamamoto, T. Kawaguchi, T. Yoshino, M. Imaeda, Efficient 340-nm light generation by a ridge-type waveguide in a first-order periodically poled MgO:$LiNbO_3$, Opt. Lett. 28 (2003) 1344–1346.
[84] Y. Nishida, H. Miyazawa, M. Asobe, O. Tadanaga, H. Suzuki, Direct-bonded QPM-LN ridge waveguide with high damage resistance at room temperature, Electron. Lett. 39 (2003) 609–611.
[85] J.D. Bierlein, A. Ferretti, L.H. Brixner, W.Y. Hsu, Fabrication and characterization of optical waveguides in $KTiOPO_4$, Appl. Phys. Lett. 50 (1987) 1216–1218.
[86] D. Eger, M. Oron, M. Katz, A. Reizman, G. Rosenman, A. Skliar, Quasi-phase-matched waveguides in electric field poled, flux grown $KTiOPO_4$, Electron. Lett. 33 (1997) 1548–1550.
[87] B. Agate, E.U. Rafailov, W. Sibbett, S.M. Saltiel, P. Battle, T. Fry, E. Noonan, Highly efficient blue-light generation from a compact, diode-pumped femtosecond laser by use of a periodically poled KTP waveguide crystal, Opt. Lett. 28 (2003) 1963–1965.
[88] M. Rusu, E.U. Rafailov, R. Herda, O.G. Okhotnikov, S.M. Saltiel, P. Battle, S. McNeil, A.B. Grudinin, W. Sibbett, Efficient generation of green and UV light in a single PP-KTP waveguide pumped by a compact all-fiber system, Appl. Phys. Lett. 88 (2006) 121105.
[89] E.U. Rafailov, D.J.L. Birkin, W. Sibbett, P. Battle, T. Fry, D. Mohatt, Efficient frequency doubling of a pulsed laser diode by use of a periodically poled KTP waveguide crystal with Bragg gratings, Opt. Lett. 26 (2001) 1961–1962.
[90] S.J.B. Yoo, R. Bhat, C. Caneau, M.A. Koza, Quasi-phase-matched second-harmonic generation in AlGaAs waveguides with periodic domain inversion achieved by wafer-bonding, Appl. Phys. Lett. 66 (1995) 3410–3412.
[91] X. Yu, L. Scaccabarozzi, O. Levi, T.J. Pinguet, M.M. Fejer, J.S. Harris, Templated design and fabrication for low-loss orientation-patterned nonlinear AlGaAs waveguides pumped at 1.55 μm, J. Crystal Growth 251 (2003) 794–799.
[92] Z. Ye, Q. Lou, J. Dong, Y. Wei, L. Lin, Compact continuous-wave blue lasers by direct frequency doubling of laser diodes with periodically poled lithium niobate waveguide crystals, Opt. Lett. 30 (2005) 73–74.
[93] K. Sakai, Y. Koyata, Y. Hirano, Planar-waveguide quasi-phase-matched second-harmonic-generation device inY-cut MgO-doped $LiNbO_3$, Opt. Lett. 31 (2006) 3134–3136.
[94] K.P. Petrov, A.T. Ryan, T.L. Patterson, L. Huang, S.J. Field, D.J. Bamford, Spectroscopic detection of methane by use of guided-wave diode-pumped difference-frequency generation, Opt. Lett. 23 (1998) 1052–1054.
[95] M.A. Arbore, M.M. Fejer, Singly resonant optical parametric oscillation in periodically poled lithium niobate waveguides, Opt. Lett. 22 (1997) 151–153.
[96] G. Schreiver, D. Hofmann, W. Grundkoetter, Y.L. Lee, H. Suche, V. Quiting, R. Ricken, W. Sohler, Nonlinear integrated optical frequency converters with periodically poled Ti:$LiNbO_3$ waveguides, Proc. of SPIE 4277 (2001) 144–160.
[97] X. Xie, A.M. Schober, C. Langrock, R.V. Roussev, J.R. Kurz, M.M. Fejer, Picojoule threshold, picosecond optical parametric generation in reverse proton-exchanged lithium niobate waveguides, J. Opt. Soc. Am. B 21 (2004) 1397–1402.
[98] C. Langrock, S. Kumar, J.E. McGeehan, A. Willner, M.M. Fejer, All optical signal processing using χ^2 nonlinearities in guided-wave devices, J. Lightwave Tech. 24 (2006) 2579–2592.
[99] S. Tanzilli, H. De Riedmatten, H. Tittle, H. Zbinden, P. Baldi, M. De Micheli, D.B. Ostrowsky, N. Gisin, Highly efficient photon-pair source using periodically poled lithium niobate waveguide, Electron. Lett. 37 (2001) 26–28.
[100] C. Langrock, E. Diamanti, R.V. Roussev, H. Takesue, Y. Yamamoto, M.M. Fejer, Highly efficient single-photon detection at communication wavelengths by use of upconversion in reverse-proton-exchanged periodically poled $LiNbO_3$ waveguides, Opt. Lett. 30 (2005) 1725–1727.
[101] S. Tanzilli, W. Tittel, M. Halder, O. Alibart, P. Baldi, N. Gisin, H. Zbinden, A photonic, quantum information interface, Nature 437 (2005) 116–120.
[102] S. Tanzilli, W. Tittel, H. De Riedmatten, H. Zbinden, P. Baldi, M. De Micheli, D.B. Ostrowsky, N. Gisin, PPLN waveguide for quantum communication, Eur. Phys. J. D 18 (2002) 155–160.

[103] P.E. Powers, T.J. Kulp, S.E. Bisson, Continuous tuning of a continuous-wave periodically poled lithium niobate optical parametric oscillator by use of a fan-out grating design, Opt. Lett. 23 (1998) 159–161.
[104] G. Imeshev, M. Proctor, M.M. Fejer, Phase correction in double-pass quasi-phase-matched second-harmonic generation with a wedged crystal, Opt. Lett. 23 (1998) 165–167.
[105] I. Juwiler, A. Arie, A. Skliar, G. Rosenman, Efficient quasi-phase-matched frequency doubling with phase compensation by a wedged crystal in a standing-wave external cavity, Opt. Lett. 24 (1999) 1236–1238.
[106] G. Imeshev, M. Proctor, M.M. Fejer, Lateral patterning of nonlinear frequency conversion with transversely varying quasi-phase-matching gratings, Opt. Lett. 23 (1998) 673–675.
[107] J.R. Kurz, A.M. Schober, D.S. Hum, A.J. Saltzman, M.M. Fejer, Nonlinear physical optics with transversely patterned quasi-phase-matching gratings, IEEE J. Sel. Top. Quant. Electron. 8 (2002) 660–664.
[108] K. Kintaka, M. Fujimura, T. Suhara, H. Nishihara, Third harmonic generation of Nd:YAG laser light in periodically poled $LiNbO_3$, Electron. Lett. 33 (1997) 1459–1461.
[109] W.R. Bosenberg, J.I. Alexander, L.E. Myers, R.W. Wallace, 2.5-W, continuous-wave, 629-nm solid-state laser source, Opt. Lett. 23 (1998) 207–209.
[110] M. Nazarathy, D.W. Dolfi, Spread-spectrum nonlinear-optical interactions: quasi-phase matching with pseudorandom polarity reversals, Opt. Lett. 12 (1987) 823–825.
[111] M.A. Arbore, O. Marco, M.M. Fejer, Pulse compression during second-harmonic generation in aperiodic quasi-phase-matching gratings, Opt. Lett. 22 (1997) 865–867.
[112] G. Imeshev, M.A. Arbore, M.M. Fejer, A. Galvanauskas, M. Fermann, D. Harter, Ultrashort-pulse second harmonic generation with longitudinally nonuniform gratings: Pulse compression and shaping, J. Opt. Sci. Am. B 17 (2000) 304–318.
[113] M.H. Chou, K.R. Parameswaran, M.M. Fejer, I. Brener, Multiple channel wavelength conversion using engineered quasi-phasematching structures in $LiNbO_3$ waveguides, Opt. Lett. 24 (1999) 1157–1159.
[114] A. Arie, K. Fradkin-Kashi, A. Bahabad, G. Rosenman, P. Urenski, Multiple nonlinear processes in 1D and 2D periodic and quasi-periodic structures, Proc. SPIE 4972 (2003) 13–24.
[115] M. Asobe, O. Tadanaga, H. Miyazawa, Y. Nishida, H. Suzuki, Multiple quasi-phase-matched $LiNbO_3$ wavelength converter with a continuously phase-modulated domain structure, Opt. Lett. 28 (2003) 558–560.
[116] S. Zhu, Y. Zhu, Y. Qin, H. Wang, C. Ge, N. Ming, Experimental realization of second harmonic generation in a Fibonacci optical superlattice of $LiTaO_3$, Phys. Rev. Lett. 78 (1997) 2752–2755.
[117] X. Liu, Y. Li, Optimal design of DFG-based wavelength conversion based on hybrid genetic algorithm, Opt. Express 11 (2003) 1677–1688.
[118] J. Huang, X.P. Xie, C. Langrock, R.V. Roussev, D.S. Hum, M.M. Fejer, Amplitude modulation and apodization of quasi-phase-matched interactions, Opt. Lett. 31 (2006) 604–606.
[119] N.G.R. Broderick, G.W. Ross, H.L. Offerhaus, D.J. Richardson, D.C. Hanna, Hexagonally poled lithium niobate: A two-dimensional nonlinear photonic crystal, Phys. Rev. Lett. 84 (2000) 4345–4348.
[120] A.M. Weiner, A.M. Kan'an, D.E. Leaird, High-efficiency blue generation by frequency doubling of femtosecond pulses in a thick nonlinear crystal, Opt. Lett. 23 (1998) 1441–1443.
[121] M.A. Arbore, O. Marco, M.M. Fejer, Pulse compression during second-harmonic generation in aperiodic quasi-phase-matching gratings, Opt. Lett. 22 (1997) 865–867.
[122] K. Green, A. Galvanauskas, K.K. Wong, D. Harter, Cubic-phase mismatch compensation in femtosecond CPA systems using nonlinear-chirp-period poled $LiNbO_3$, in: Nonlinear Optics: Materials, Fundamentals, and Applications, Technical Digest, 2000, pp. 113–115.
[123] M.A. Arbore, A. Galvanauskas, D. Harter, M.H. Chou, M.M. Fejer, Engineerable compression of ultrashort pulses by use of second-harmonic generation in chirped-period-poled lithium niobate, Opt. Lett. 22 (1997) 1341–1343.
[124] G. Imeshev, M.M. Fejer, A. Galvanauskas, D. Harter, Pulse shaping by difference-frequency mixing with quasi-phase-matching gratings, J. Opt. Soc. Am. B 18 (2001) 534–539.
[125] G. Imeshev, M.M. Fejer, A. Galvanauskas, D. Harter, Generation of dual-wavelength pulses by frequency doubling with quasi-phase-matching gratings, Opt. Lett. 26 (2001) 268–270.
[126] A.M. Schober, G. Imeshev, M.M. Fejer, Tunable-chirp pulse compression in quasi-phase-matched second-harmonic generation, Opt. Lett. 27 (2002) 1129–1131.
[127] L. Gallmann, G. Steinmeyer, G. Imeshev, J.P. Meyn, M.M. Fejer, U. Keller, Sub-6-fs blue pulses generated by quasi-phase-matching second-harmonic generation pulse compression, Appl. Phys. B: Lasers and Optics B 74 (2002) S237–S243.
[128] I. Jovanovic, B.J. Comaskey, C.A. Ebbers, R.A. Bonner, D.M. Pennington, E.C. Morse, Optical parametric chirped-pulse amplifier as an alternative to Ti:sapphire regenerative amplifiers, Appl. Opt. 41 (2002) 2923–2929.
[129] M. Charbonneau-Lefort, A.M. Schober, B. Afeyan, M.M. Fejer, Broadband optical parametric amplifier using chirped quasi-phase-matched gratings, in: Conf. on Lasers and Electro-Optics, 2006, CThO2.
[130] D. Artigas, D.T. Reid, M.M. Fejer, L. Torner, Pulse compression and gain enhancement in a degenerate optical parametric amplifier based on aperiodically poled crystals, Opt. Lett. 27 (2002) 442–444.
[131] M. Charbonneau-Lefort, M.M. Fejer, B. Afeyan, Tandem chirped quasi-phase-matching grating optical parametric amplifier design for simultaneous group delay and gain control, Opt. Lett. 6 (2005) 634–636.